Journal Name

Dynamic Article Links ►

Cite this: DOI: 10.1039/c0xx00000x

www.rsc.org/xxxxxx

ARTICLE TYPE

Large directional conductivity change in chemically stable layered thin films of vanadium oxide and a 1D metal complex

C. Glynn[a,b], D. Thompson[b], J. Paez[c], G. Collins[a,d], E. Benavente[e,f], V. Lavayen[g], N. Yutronic[h], J. D. Holmes[a,b,d], G. González[f,h], and C. O'Dwyer[a,b,i]*

Received (in XXX, XXX) Xth XXXXXXXXX 20XX, Accepted Xth XXXXXXXXX 20XX
DOI: 10.1039/b000000x

Electroactive hybrid and layered oxides and related materials, where the inorganic phase is the host, offer the conductivity characteristics of semiconductors, has led to their use in thin film transistors and related electronic devices where the host-guest interaction offered conductivity with improved processability. We describe the synthesis and characterization of a nanocomposite that shows large conductivity anisotropy when deposited as a thin film. We made the material by inserting quasi 1-dimensional potassium tetracyanoplatinate metal complexes with insulating electrical properties in between stacked nanosheets of vanadium oxide xerogels. Detailed structural and compositional analysis using transmission electron microscopy and X-ray photoelectron spectroscopy confirms that the hybrid material forms from a topotactic reaction and the framework of the layered host oxide structure is maintained. The hybrid film demonstrates a ~1000-fold conductivity change between transport parallel and perpendicular to the film at room temperature. Temperature dependent transport measurements confirm Ohmic conduction perpendicular to the stack and small polaron hopping conduction parallel to the layering direction of the film. The conductivity anisotropy and simple synthesis demonstrates that nanostructured layered hybrids can provide alternative materials for thin film complimentary logic and resistive memory.

1. Introduction

One-dimensional conductive partially oxidized platinum polymers have been shown to have a linear chain arrangement in which the dz electron orbital of the metal atoms overlap, allowing extended electron delocalization in one dimension[1, 2]. Within this class of quasi-one dimensional solids (Q1-D) the most well-known tetracyanoplatinate is $K_2Pt(CN)_4Br_{0.3}$ (Krogmann's salt, Fig. 1, platinum potassium tetracyanoplatinate) behaves as a one-dimensional metal at room temperature; without the Br, it has a strongly insulating character[2]. Incorporating this class of linear complexes, of which the tetracyano complex $[M(CN)_4]$ is a prime example, into conductive host materials could offer synthetic routes to electronic complexes in which the magnitude and mechanism of the conductivity is controlled by the degree of metal atom orbital overlap. These kinds of structural arrangements could be realized in hybrid materials where metal quantum effects such as Luttinger liquid behaviour[3, 4], Peierl's transitions[5] and charge density waves are mixed with various conduction mechanisms found in host materials[6]. $K_2Pt(CN)_4$ is a known and useful compound in the chemistry of platinum complexes[7], and has potential uses in new kinds of electrical circuitry based on nanoscale building blocks[8], where the metal-metal bonds can regulate the electrical and mechanical properties of the units.

In regular insulators, semiconductors and metals, the electronic response is almost independent of direction whereas in Q1-D solids enhanced electronic response occurs in specifically one direction, along the axial length of the chain via a Peierls distortion and associated transition[9]. In particular, interactions between transition metal oxides and Q1-D linear chains of metal complexes can form layered materials with complex conduction characteristics[10, 11], where the intercalation of the metal is known to enhance, affect or even suppress CDW observation[12] and strongly correlated electronic effects.

When the building blocks of an electronic material consist of an inorganic and an organic phase where the resulting structure and properties are strongly correlated to their interaction[13-18]. A judicious choice of organic and inorganic phases (semiconducting, self-assembling, intercalating, insulating, passivating) can allow rational design for added functionality[19, 20]. The resulting hybrid structure can be well defined[13, 21, 22] with strong, specific organic-inorganic and organic-organic interfaces. Integrating layered nanostructures in their 1D form into electronic devices[23] may expand the field of advanced materials for electronics[24]. For example, the versatile redox-dependent electronic properties and intercalation properties of vanadium oxide[25] and related materials[26], has fostered its use in numerous applications in catalysis[27], Li- and Na-ion batteries[28, 29], electrochromic materials, field-effect transistors (FETs)[30] and photoconductors[31], gas sensors, spintronic and piezoelectric devices[32], actuators[33] and others[34]. Previous investigations of hybrid organic-inorganic vanadium oxide-based structures[35] and single phase vanadium oxide thin films[36] have shown that polaron hopping conduction[37]

through the oxide is maintained, but the organic phase offers mainly structural modifications rather than a direct influence on electronic conduction characteristics[38-40]. Improvements in thin film growth and deposition methods, together with strongly correlated electronic behaviour in transition metals including metal-insulator transitions[39, 40], make multivalent oxides potentially very useful for technology applications[41-44]. Vanadium oxides are being considered as oxide semiconductor channel materials and have demonstrated a promising degree of electrostatic control and gating effects[45, 46] in the metal-insulator transition[47, 48] for switches and logic elements using VO_2.

We show here how Q-1D linear chain metal complexes can form vanadium oxide electronic material similar to an intercalated V_2O_5 xerogels[21, 49-53], with excellent long term chemical and structural stability. The Q1-D complex is posited to be placed between n-type conducting V_2O_5 sheets, and we show using detailed microscopy and spectroscopy that a topochemical reaction maintains the host structure. We demonstrate, that the hybrid exhibits strong conductivity anisotropy at room temperature and importantly, without a phase change of the V_2O_5. A >1000-fold conductivity flip occurs depending on whether electronic conduction is along the film or through the thickness of thin film. Our results demonstrate that the conduction flip is due to a switch between higher conductivity polaronic transport along the film layers (parallel to the substrate) and much more resistive Ohmic transport perpendicular to the stack, caused by the presence of the Q1-D chains. Spectroscopic analyses confirm that the material remains chemically and structurally stable for at least a period of >2 years.

2. Experimental section

Microwave-assisted hydrolysis of orthorhombic V_2O_5 with *t*-butyl alcohol[54, 55] was accomplished using a frequency of 1.225 Ghz pulsed with a period of 30 s for 1 h. To synthesize $K_2[Pt(CN)_4]$, 1.0 g of $K_2Pt(Cl)_4$ was dissolved in 150 mL of water. Subsequently, 4 equiv. of KCN were added in small portions for 15 mins. Within an hour the initially red solution became colourless. The resulting solid was dissolved in a minimum volume of water at 338 K and placed in an ice bath. The white needle-like crystals that formed were filtered and washed with water. The intercalation product was obtained by mixing $K_2[Pt(CN)_4]$ with V_2O_5 xerogel in a molar ratio 0.5:1 (1.83×10^{-4} mol of $K_2[Pt(CN)_4]$ in 3.66×10^{-4} mol of V_2O_5). This resulted in the formation of the bourbon red precipitate product which was separated from the supernatant solution, centrifuged and dried at room temperature, and stored in an argon environment.

X-ray powder diffraction characterization was performed using a SIEMENS D5000 diffractometer (Cu-Kα, λ=1.5418 Å, operation voltage 40 kV, current 30 mA). The scanning electron microscopy (SEM) analysis was performed using a Hitachi S4800 FESEM. Chemical composition was determined by elemental chemical analysis (SISONS model EA-1108), and thermal analysis (TA) was conducted in a NETZSCH Model STA 409 thermogravimetric system with a microprocessor driven temperature control unit and a TA data station from 273 to 823 K at 10 K min^{-1}.

Transmission electron microscopy (TEM) was conducted using a JEOL 2100F FEGTEM and a JEOL 2011 TEM operating at 200 kV. X-ray photoelectron spectroscopy was performed using a Kratos Axis 165 equipped with a monochromatic Al source (Kα 1486.58 eV) with a spot size of 1 mm. The source power was 150 W.

Raman scattering measurements were conducted using a Horiba Dilor XY LabRAM spectrometer equipped with an Olympus BX40 confocal microscope. Excitation was provided by a 633 nm He–Ne laser. The spectra were typically acquired with a 5 s exposure time and a laser power density <45 μW $μm^2$.

Electrical conductivity measurements were taken in central regions formed from a consistent drying line and deposition thickness, away from thinner edges. For detail on effects of withdrawing from sol-gel solutions, see Ref. [56]. Briefly, viscous composite sol-gel is extruded at fixed rate from a source sol at an angle. Tear-drop deposits at the electrode edges were ignored. Layers were made intentionally thick (~500 nm - 5 μm) so that top contacts using 4-probe measurements and side contacts (involving the intercalated complexes) were electrically addressable. Gold wire was contacted to the surface using conductive gold paste. Bottom contacts were made for perpendicular charge transport through the film and 2- and 4-probe measurement along the layering direction of the thin film deposit. A gold-coated glass covered in a Si_3N_4 membrane was lithographically defined to have 4 nodules of gold exposed on the substrate. I-V curves and temperature-dependent conductivity measurements were made using a Keithley 2420 dc voltage source and an Agilent 34401A Digital Multimeter in a Faraday cage.

3. Results and discussion

3.1 Electrical conduction anisotropy in V_2O_5/Q1-D thin film stacks

First, we detail the strongly anisotropic electrical characteristics of the Q1-D-vanadium oxide thin films and subsequently correlate these findings to a detailed structural analysis of the hybrid thin film. In the first experiment, 2-probe measurements were made from side-contacting the vanadium oxide, so the influence of the metal complex within the conducting framework could be established. Figure 1a,b shows the corresponding I-V curves at room temperature, and we note that the profile follows a symmetrical thermionic emission-like profile with symmetry in the forward and reverse bias current where all conducting sheets are electrically addressed. Figure 1b shows the I-V curves for direct conductivity measurements through the film thickness (by comparison to measurements along the film where all the layers are addressed). Figure 1c shows the molecular structure of the V_2O_5 layers and the Q1-D metal complex.

We observe a large anisotropy in overall conductivity, with a ~1000-1300× decrease (from 3.2×10^{-2} S cm^{-1} to $<5 \times 10^{-5}$ S cm^{-1}) in conductivity perpendicular to the layering for a deposit that is 5 μm thick compared to conductivity along the plane of the deposit. The response is linear (Ohmic) indicating that the stack is less sensitive to the polaron hopping mechanism through the vanadium oxide framework itself. We attributed this anisotropy to the presence and blocking conduction characteristics of the intercalated Q1-D metal complex solid between the nanosheets of V_2O_5 of the crystallized sol-gel deposit. Control measurements of the conductivity of the pristine xerogel in both directions (parallel and perpendicular), shown in Supplementary material Fig. S1,

shows only a small variation in conductivity with no change in the mechanism of charge transport for similarly thick deposits. Uniquely, with the complex intercalated, perpendicular transport is Ohmic and far more resistive. As will be detailed in subsequent sections, this material is not simply a mixture of both the Q1-D and V_2O_5; a strong host-guest interaction maintains the layered structure of the xerogel, with the Q1-D complex dominating charge transport perpendicular to the layering.

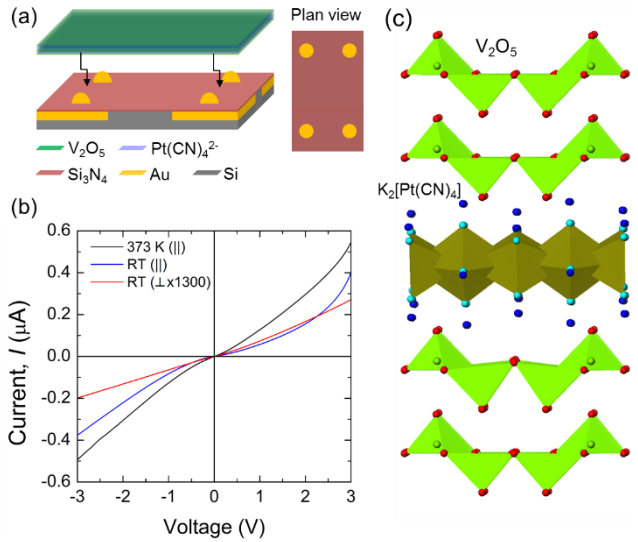

Fig. 1 Schematic arrangement for transport measurements of the $K_2[Pt(CN)_4]_{0.03}V_2O_5$ thin film. (b) I-V curves acquired parallel to (along) the film at RT and 373 K, and perpendicular to the thin film at RT. (c) CPK model of an intercalated structure with the Q1-D molecule oriented along the *a*-axis of the V_2O_5 unit cell. The structure is drawn as polygons.

Variations of 100-1000× have been reported in macroscopic cm-sized organic-inorganic materials compressed into highly disordered pellets where inter-grain boundaries alter the effective conduction pathways[57, 58]. Other techniques include using poly (ethylene oxide) (PEO) or the oxide hydration states to widen the gap between V_2O_5 layers, but for deposits encapsulated with sheaths of polymer[59]. Here, the 1-dimensional solids of insulating nature allow large directional conduction anisotropy while leaving the deposit as a thin film, unaltered mechanically or physically. As the oxide film is fully aged, increases in conductivity that are known to occur during ageing over a period of years, are avoided. By designing a 4-probe contact area on an insulating substrate (see Fig. 1a), and similarly on the top of the resulting deposit, we were able to probe temperature dependent conductivity along and through the thin film, while extracting the contribution of contact resistance to the deposit. The intrinsic resistance along the stack is 13.2 MΩ, and the contact resistance is 0.56 MΩ. An intrinsic conductivity of 2.9 – 5.0 × 10^{-2} S cm^{-1} was obtained for several nanosheets stacks, typically of 500 nm -5 μm thickness. Through the thickness of the deposit however, 4-probe data confirm the 2-probe measurements where a ~1000-fold reduction in conductivity is found. Along the stack, the conductivity is marginally higher than bulk V_2O_5 but of the same order of magnitude, while showing a large anisotropy perpendicular to the layers.

The transport in both directions was also measured in the range 77 – 400 K, but kept below temperatures where a metal-insulator transition or other thermalized effects involving electron-phonon coupling in V_2O_5 would complicate the effect of the intercalated Q1-D complex. Typically, polaron hopping transport (conductivity) in vanadium oxides follows a power law according to $\sigma = \sigma_0 \exp -(T_0/T)^{\beta}$, where T_0 is a measure of the electronic disorder in the film. The value of β was estimated following the approach of Bharadwaja *et al.*[36] to be in the range 0.23 – 0.27, consistent with 2D Mott variable range hopping (VRH) conduction.

Figure 2 shows the data plotted in accordance with a variable range hopping model with $\beta = 0.25$ for transport along the layering direction. Measurements were made using 4-probe measurements by contacting alternate pairs of electrodes.

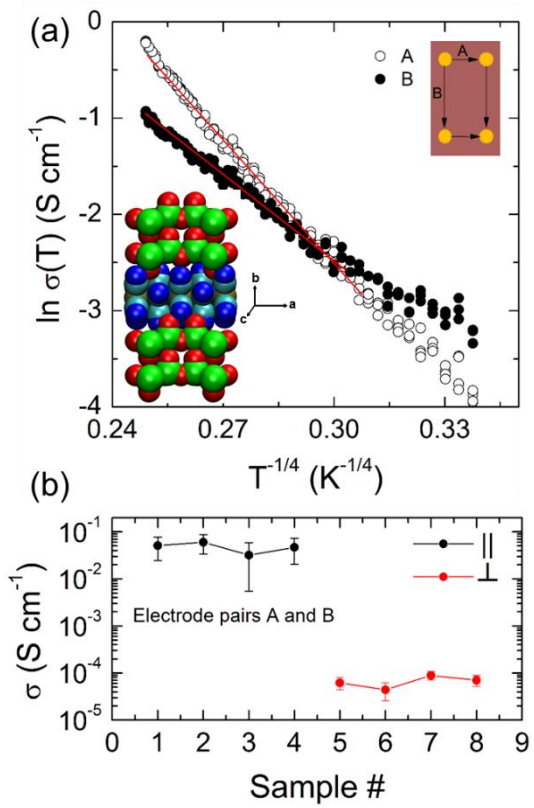

Fig. 2 (a) Variation in conductivity with temperature in the range 77 – 400 K for Q1-D intercalated V_2O_5 thin film stacks. The inset show a CPK space-filling model of the Q1-D intercalated V_2O_5 with the Pt-Pt bond axis parallel to the *a*-axis of V_2O_5. (b) Conductivity determined from 2-probe devices for electrode pairs A and B parallel to the layering direction and 2-probe data acquired through the thin film stack. Each data point is an average of 20 measurements for each direction from 4 separate samples.

The consistency shows that directional resistance change is not found in-plane. For variable range hopping in transition metal oxides[60] with multivalent impurities, the conductivity based on carriers hopping a distance *R* from occupied levels to adjacent, vacant ones without any applied potential or field, is approximated by

$$\ln \sigma = \ln\left(\frac{\upsilon_0 e^2 C(1-C)}{kRT}\right) + \left(2\alpha R - \frac{E_{hop}}{kT}\right) \qquad (1)$$

where α is the inverse localization length of a charge carrier, υ_0 is the phonon frequency, C is the concentration ratio $V^{4+}/(V^{4+} + V^{5+})$, and E_{hop} is the energy associated with a polaron hop from occupied

to free energy levels, separated by a distance *R*. Fitting Fig. 2 shows more than one slope, leading to a dispersion of activation energies for Q1-D intercalated V_2O_5 in the range $E_{hop} \sim 0.19 - 0.24$ eV parallel to the layering over the temperature range investigated, which is consistent with 2D Mott-like theory.[61] Unlike the xerogel, this hybrid has Q1-D complex chains in specific locations throughout the structure, which we suggest based on measurements detailed below, are intercalated into the host matrix. While the packing density of the Q1-D chains is not known, preferential electronic texturing whereby the majority of intercalated chains, such as those horizontally aligned along the *a*-axis of the V_2O_5 unit cell, could account for the small variation in hopping exponents in-plane, as shown in Fig. 2a, although detailed molecular dynamics and periodic density functional theory calculations would need to be employed to probe this effect in detail.

We do note, however, that other VRH conduction mechanisms could apply,[37, 62] specifically when considering the Coulomb interactions between localized charges arising from multiple valence states. Since wavefunction overlap is possible in closely spaced multivalent vanadium centers, Anderson localization[63] is likely not a factor and no Coulomb gaps exists that hinder the probability of polaron formation and hopping of charges. The range of exponents almost spans the 3D and 2D Mott-like theories, and we believe this is related to the inclusion of the insulating Q1-D metal complex chains; the xerogel without any intercalants has a characteristic 3D Mott character. However, for $\beta = 0.25$ or very close to it, variable range hopping occurs through a constant 2D density of states. For measurements that have exponents larger than 0.25, the likelihood is that the reduction of the V_2O_5 (and thus site to site impurity concentration) is not identical at the molecular level throughout a deposit of several cms in surface area. Changes in hopping distances could arise if the degree of Q1-D packing was either reduced or non-uniform in places throughout the interlayer spacing. As will be shown below, some regions of the thin film are locally less crystalline, and we believe this contributed to the slight variations in temperature dependent (higher) conductivity parallel to the layering.

The observation of recrystallized V_2O_5 nanocrystals, detailed below, within the stable and fully aged intercalated composite can act as localized concentrated hopping sites within the V_2O_5-Q1-D nanosheet stacks, but its effect in various granular thin films, nanotubes[64], and particularly vanadium oxide has not previously been confirmed experimentally. They are ruled out as the cause of the large directional change in conductance and mechanism, which is dominated by the presence of the complex inside the xerogel. Estimates of the hopping distance *R* and the degree of disorder T_0 possible for single crystal materials show large discrepancies particularly where the conduction is governed by material parameters (for simple and more complex host-guest systems) that are not inherent in the definition of T_0 ($\sim 3q^2/4\pi\varepsilon\varepsilon_0 k\alpha$); trends in the variation of *R* and the inverse localization length α are to an extent possible in some cases, but in the Q1-D-intercalated V_2O_5 films here, the determination is complicated without detailed knowledge of the particular molecular structure of the host-guest system, its effective dielectric constant, etc.

The temperature dependence gives information on the mechanisms of conduction in general and we performed these measurements to determine if the large anisotropy in conductivity or resistivity through a thin film deposit follows a similar mechanism for V_2O_5. The transport through the deposit, from Fig. 1b, is Ohmic with high average resistances ($\sim 5 \times 10^{-5}$ S cm^{-1}), which give much lower (3 orders of magnitude) conductivity compared to conduction along the plane, as shown in Fig. 2b. The conduction mechanism and values along the more conductive V_2O_5 2D nanosheets that periodically stack to make up the film, are more or less independent of the 2-and 4-probe conduction direction (Fig. 2a). Thus, the insertion of insulating Q1-D complexes results in a very large conductivity reduction when transport is perpendicular to the thin film, while current flow maintains a polaronic hopping conduction through the layers of vanadium oxide, when the Q1-D complex is present. The Ohmic and highly resistive transport perpendicular to the film has implications for bipolar switching behaviour that is not sensitive to non-linearity or rectification. Without the Q1-D complex, no directional conductivity flip is observed, and the conductance and transport mechanism along and through the pristine xerogel remain similar. Next, we describe a detailed investigation of the structure and crystallinity of the vanadium oxide oxide sheets with the Q1-D complex, so that a correlation between the directional electrical response and the structure can be determined.

3.3 Formation of stable, ordered Q1-D functionalized layered thin films

For many electronic investigations of thin films, the detailed structural analysis is often limited, which reduces the usefulness of the electronic data for rational design when the functional property is strongly dictated by the fine details of the structure. Here, it is critical to define the structural effect of the Q1-D complex on the nanosheets of crystalline V_2O_5. The layer spacing of the dry xerogel material, with formula $V_2O_5{\cdot}0.5H_2O$ is known to be ~8.7 Å from extensive diffraction and spectroscopic analyses[21, 65]. V_2O_5 is a disordered n-type semiconductor with insulating character defined by a band gap reported to be in the range ~2.25-2.3 eV. It crystallizes in an orthorhombic crystal structure (space group *Pmmn*), with lattice constants determined to be a = 1.15 nm, b = 0.36 nm, and c = 0.44 nm. It is well established that this interlaminar spacing, formed between the bilayered arrangement of edge shared VO_5 units[66, 67] propped apart by weak van der Waals forces (Fig. 1), varies as a function of the mole fraction of the water in the hydrated xerogel[68]. We specifically added 1 mole of crystal water to the xerogel to create $V_2O_5{\cdot}1.5H_2O$ to trigger an expansion of the lamellar structure resulting in an increase in the layer spacing to 12.3 Å. As will be shown through more sensitive Raman scattering data, these spacings remained consistent for samples stored for a period of >2 years. The (00*l*) peaks in Fig. 3 indicate a superlattice of V_2O_5 layered slabs for the xerogel and the intercalated compound. Following correction for Lorentz polarization, Compton scattering and material absorption effects, the metal complex intercalated xerogel is found to maintain a similar overall layered structure. Low-angle XRD confirms Bragg reflections stemming from X-ray path length differences with a 12.3 Å spacing between lowest angle (00*l*) planes; this defines the expected interlayer spacing for the starting xerogel host.

$K_2[Pt(CN)_4]$ is described crystallographically by the space group P*bcn*[69] by neutron diffraction; the crystal structure consists of nearly square planar $Pt(CN)_4^{2-}$ groups stacked parallel to the *c*-

axis forming linear chains of Pt atoms (Fig. 3)[70]. We noticed that the use of a solvent disrupts the lattice, resulting in a change of Pt-Pt separation. However, when the solvent is removed, the initial colour of the complex is restored and the lattice parameters of the complex are identical to the original lattice parameters; any changes are expected then to come from interactions with the host material. In the case of the $K_2[Pt(CN)_4]$ hydrate, simply allowing the freshly recrystallized yellow/green solid to dry on the countertop results in a slow change of the colour to white[70]. The colour of the $K_2[Pt(CN)_4]$ used in the synthesis was white, where the range of separation of Pt-Pt bonds is 3.1-3.7 Å, and the maximum for the optical absorption band ranges from 600 to 283 nm; Pt-Pt complexes with interatomic separations greater than 3.7 Å are typically colorless.

After the intercalation reaction, the XRD pattern of the $K_2[Pt(CN)_4]_{0.03}V_2O_5$ nanocomposite (in Fig. 3) shows a good degree of layering, consistent with its host and indicative of a topotactic intercalation reaction. The overwhelming majority of organic or other species inserted into vanadium oxide[68, 71] and a range of other layered double hydroxides and transition metal oxides[17, 51] results in the widening of the interlayer spacing[72].

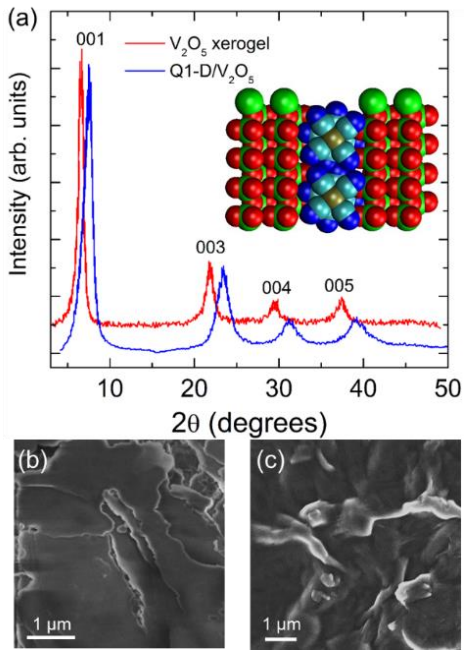

Fig. 3 (a) X-ray diffraction patterns for V_2O_5 and $K_2[Pt(CN)_4]_{0.03}V_2O_5$ acquired in Bragg-Bretano geometry showing periodic Bragg reflections from the V_2O_5 layered materials. The inset to (a) shows a CPK space-filling model of the layered structure with the Q1-D molecule oriented along the *c* axis of the V_2O_5 unit cell. (b,c) SEM images of the $K_2[Pt(CN)_4]_{0.03}V_2O_5$ and initial V_2O_5 xerogel confirming its deposition.

When measured, we find that the interlayer spacing of the composite is ~11.2 Å which is marginally less than the host xerogel. Additionally, the number and periodicity of reflection harmonics and the consistency in FWHM of the (00*l*) peaks confirms that the thickness of the V_2O_5 layers remains similar; the angle shift implies a narrower distance between self-similar layers after addition of the Q1-D complex. The net contraction of ~1.1 Å, however, can be affected by the mole fraction of water, and so is not likely to be dominantly affected by the intercalation of the Q1-D complex, and may stem from a range of other possible species such as $[K(H_2O)_6]^+$ or $[Pt(CN)_6]$ clusters. Dehydration and some guest species have been previously shown to reduce the interlayer spacing in vanadium oxide bronzes[73].

The diffraction patterns shown in Fig. 3(a) exhibit characteristic double bi-layer reflections (absence of the (002) reflection)[74] which confirms that intercalation of the Q1-D complex maintains the layered order of the host; all peaks shift by an identical amount to lower angles in the composite. An SEM image of the final product is shown in Fig. 3b, which maintains the overall morphology of the starting xerogel (Fig. 3c). The CPK models in Fig. 3a show that the Q1-D chain with their Pt-Pt chains along the *a*-axis of V_2O_5 can insert into the interlayer spacing of the xerogel so that the pillared square CN groups slot between vanadyl oxygen groups of the V_2O_5 lattice, which avoids a widening of the interlayer spacing. In spite of a low amount of intercalated guest, the diffraction pattern maintains the same form, indicating a relatively strong host-guest interaction[75], enough to produce a pillaring effect between layers or sheets of the V_2O_5 and avoids exfoliation or puckering of the layered matrix after intercalation. Although the intercalation ability of known cyanide species is not well documented, we have previously confirmed intercalation of polyacrylic acid (PAN) in its colloidal form (due to a low solubility of this polymer) in other 2D matrices such as MoS_2 [76] and in a lamellar clay (bentonite)[77]. In the interlayer spacing, PAN forms cylindrical arrangements of about 6 nm diameter, defining a conformation similar to that found in the tetracyanoplatinate. Interestingly, the intercalation of PAN into MoS_2 is possible directly without any activated intermediate as usually occurs in that chemistry.

Thermogravimetric analysis shown in Fig. 4 shows that a 4.4% weight loss occurs for the intercalated material at 90 °C due to dehydration, followed by a continuous weight loss up to 152 °C. At higher temperatures the nanocomposite shows an abrupt decomposition at ~177 °C with an associated weight loss of 16%. Overall, TGA analysis suggests that cyanogen gas $(CN)_2$ is expelled and solid KCN is formed. The KCN then sublimes without decomposition at ~82 °C, based on differential thermal analysis (DTA) of the $K_2Pt(CN)_4$, shown in Fig. 4. Although the compositions of the gaseous reaction products could not be identified precisely, the percentages calculated from the thermogravimetric data indicate that 16% weight loss (at 177 °C) corresponds primarily to the extraction of loosely bound water and some crystal water.

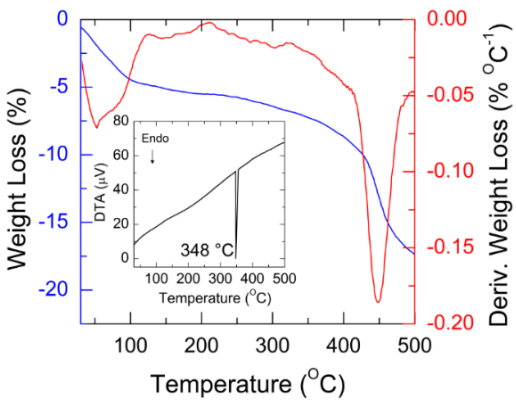

Fig. 4 Thermogravimetric analysis of the lamellar product $K_2[Pt(CN)_4]_{0.03}V_2O_5$. (Inset) Differential thermal analysis of the $K_2Pt(CN)_4$, T_g = 348–355 °C.

Figure 5 shows TEM images of flakes of the vanadium oxide xerogel prior to any intercalation reaction. The flakes were exfoliated mechanically to avoid possible adverse changes from solvent exfoliation. In Fig. 5a-c, the layered morphology is clear and the crystal structure is confirmed as orthorhombic V_2O_5. In some cases, wider spacings are found in the lattice resolved microscopy images, wider than lattice spacings for V_2O_5 of any space group (see Fig. S2). These are directly due to Moiré interference patterns[78] which arise when lattice matched stacks of 2D crystalline nanosheets with unequal spacings are overlayed, or can occur due to mistatched/misoriented sheets with equal lattice spacings. Figures 5d-f show atomic resolution images from which 1, 2 and 3 layered regions of the hybrid compound are identified. The FFT analysis indicates that no misorientation of the layers on the atomic scale is found in the regions examined, which agrees with XRD evidence of a consistent layered crystal structure and morphology in the composite.

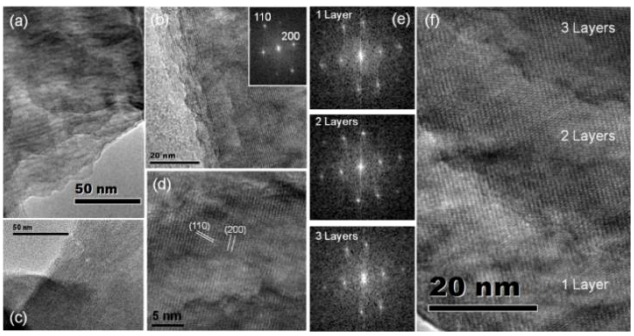

Fig. 5 (a-c) TEM images at various magnifications showing the layered structure of the V_2O_5 xerogel nanosheet stacks in transmission. The lattice fringing, electron diffraction measurements and FFT confirm the single crystalline nature and layering of the host V_2O_5 framework, stacked in the [010] direction. (d) Lattice fringes for the (200) = 0.33 nm and (110) = 0.57 nm interplanar spacings of a region composed of three hybrid layered stacks. (e,f) FFT and corresponding TEM image of the tri-period stack viewed down the *b*-axis of the unit cell showing excellent lattice matching of the V_2O_5 bilayered slabs.

Following addition of the Q1-D complex and ageing for a period of ~2 years, the resulting structure is altered. Figure 6 shows that the layered morphology is maintained and the crystal space group of the oxide remains as P*mnn*. After 2 years of ageing, the resulting structure shows some thickness variations (viewed in transmission), but the characteristic spacing between the (110) planes is maintained. Some regions of the film, however, do show reductions in crystal quality and in these regions we find through high angle annular dark field imaging (Fig. 6c,d) that V_2O_5 nanocrystallites are found randomly dispersed throughout these regions.

The composite was cast as a uniform thin film on glass to probe the structure and Raman scattering measurements were performed. In Fig. 7, we note that the original crystalline framework of the host is conserved at room temperature (the measurements were taken at laser power densities that cause negligible heating induced crystal changes[79, 80] in the V_2O_5). The influence of ageing on vanadium oxide is known[81] to result in long term complete crystallization (which is especially noted in hydrolyzed vanadium alkoxides), but these ageing effects are ignored in the majority of investigations even though this crystallization occurs over a period of months to several years, and is expected have an impact on technological development. Importantly, consistency of the inorganic phase is maintained for long periods for these electronically anisotropic thin films.

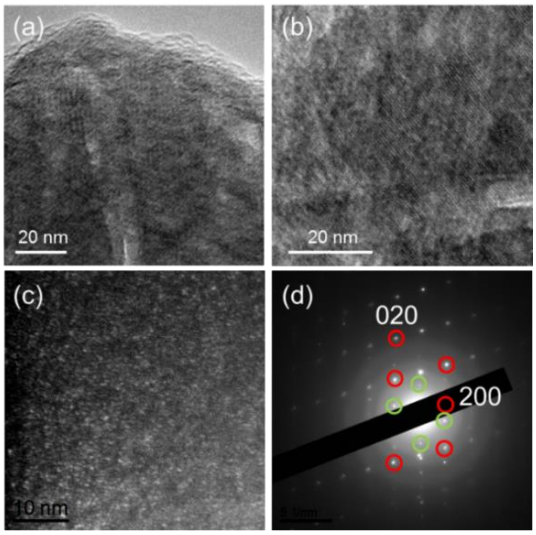

Fig. 6 (a,b) TEM images at various magnifications showing the layered structure of the intercalated nanosheet stacks in transmission. (c) STEM HAADF image of a portion of the composite showing nanocrystallites of V_2O_5 within the nanosheets. (d) Electron diffraction patterns of the crystalline layered thin film composite along the <001> zone axis and a ring pattern indexed to orthorhombic V_2O_5 nanocrystallites. Two primary crystalline orientations are found in addition to an amorphous distribution of many nanoscale (<3 nm) crystallites.

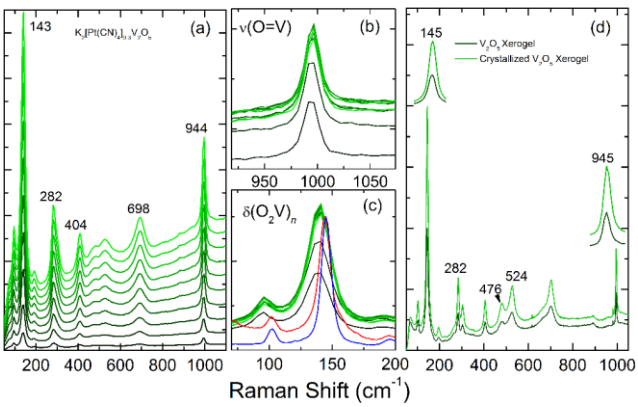

Fig. 7 (a) Raman scattering spectra of the Q1-D/V_2O_5 thin film acquired over a period of ~2 years. (b) Vanadyl phonon mode and (c) the phonon mode associated with V_2O_5 bilayer shearing. Overlayed are the corresponding modes from as-deposited and crystallized xerogel. (d) Spectra from V_2O_5 xerogel before and after thermal crystallization.

Raman scattering spectra in Figure 7 show the consistency in phonon modes from the Q1-D/V_2O_5, which are very similar to that of pure V_2O_5 xerogel. We find that after 2 years storage, the crystal structure of the vanadium oxide is fully developed. The density of reduced V^{4+} centres from the υ(O-V)-A_{1g} mode saturates (Fig. 7b). This consistent phonon mode at 994 cm^{-1} corresponds to a vibration from a V=O bond length of 0.16 nm, indicative of

V^{4+}/V^{5+} mixed valency V_2O_5, and here becomes fully defined after ageing and full crystallization[82]. The consistency in frequency in the Q1-D intercalated V_2O_5 is quite unusual, especially considering the >2 year period over which the data was captured. Notably, the frequency does not shift, which indicates a strong and stable V=O bond during ageing, with no conformation variation and consequently, no formal change in impurity center density. The ordered and lattice-matched V_2O_5 sheets remain unchanged in time with Q1-D chains intercalated between the successive stacks of V_2O_5 2D sheets. The frequency consistency is also found for the $\delta(O_2V_2)_n$ type B_{1g} + B_{3g} shear and rotational movement between the edge-shared VO_5 sub-units that make up the bilayer V_2O_5 (Fig. 7c), confirming very high layer-on-layer order at least over the 1.1 μm^2 areas probed by the laser at various points on the thin film.

Figure 7d shows Raman scattering spectra for the xerogel before and after crystallization. Upon heat treatment the spectra confirm a fully developed crystal order for the vanadium oxide stack. Rapid crystallization of xerogel thin films, however, can result in delamination of the film from the substrate. When organics or indeed the Q1-D complex here are considered, rapid crystallization of the material cannot be performed, as showing in Fig. S3, where heating (but not ageing crystallization) can result in delamination. The resulting structure of the aged $K_2[Pt(CN)_4]_{0.03}V_2O_5$ is remarkable in that it maintains a very strong resemblance to the host xerogel. The vanadyl mode (V=O) does not change in length during crystallization, where a lengthening would reduce the frequency of the mode. Thus, the Q1-D complex does not alter this bond length through reduction. We note that the rocking ρ(V=O) mode at 282 cm^{-1} is markedly affected by the Q1-D complex, by comparison to pristine xerogel. Additionally, the rocking δ(V–O–V) modes at 476 and 524 cm^{-1} are less developed when the Q1-D complex is present, even after the V_2O_5 has reached is full crystallization.

Inelastic light scattering from intermolecular vibrations give the strongest indication of the effect of the Q1-D complex on the structure of the xerogel; it primarily affects vibrations related to edge-sharing of crystal sub-units in the orthorhombic layered structure, and the displacement (but not length variation) of the vanadyl bond. Correlation to HRTEM is possible by noting the slightly higher degree of disorder in transmission and the presence of nanoscale crystallites (Fig. 6) in the Q1-D intercalated and aged xerogel. These crystallites by definition, imply a reduction in the long range order of the crystallographic *c*-axis perpendicular to the layering direction not found in the xerogel, and correlate with the larger FWHM of the 145 cm^{-1} phonon mode (and a lowering of its frequency to 143 cm^{-1} upon intercalation of the complex) of the composite compared to the xerogel in Fig. 7.

The insertion of tetracyanoplatinates into a V_2O_5 host framework allows a periodically sandwiched slab of alternating conductive and insulating materials, at the single molecular level. Its structure influences its electric properties due to its multivalent character[83], and our results shows that the composite can remain very stable over at least a couple of years. The V_2O_5 conducts via small polarons (electronic environments) associated with the V^{4+} centers in the intercalated vanadia layers. The core level binding energies for V $2p_{3/2}$, V $2p_{1/2}$ and O 1s acquired from nanosheets stacks are shown in Fig. 8 and Fig. S4. The V 2p core-levels are convoluted with two contributions each, assigned to V^{5+} (525.3 eV and 517.7 eV) and V^{4+} (524.1 eV and 516.2 eV). The hyperfine-split lines stem from strongly localized 3d electrons of isolated V^{4+} ions.

The corresponding O 1s binding energy is found at 530.7 eV from O^{2-} species with some contribution from OH^- and O^-. According to the empirical relation[84] for multivalent (variable formal oxidation states) contributions (centroid splitting) to photoelectron emission in Fig. 8, the average vanadium oxidation state in the Q1-D intercalated V_2O_5 is $\sim 13.82 - 0.68[\text{B.E.(O 1s)} - \text{B.E.(V } 2p_{3/2})] \approx 4.83$. The quantity of V^{4+} ions is typically assigned to reduction (nucleophilic uptake of oxygen by the organic species, evidentially from the shorter ~0.158 nm apical V=O bond[85]) but from Fig. 8, we observe that the presence of OH^- ions prevents a high concentration of reduced V^{4+} species typically found[86] for organic intercalated vanadium oxides; here, we surmise that the core-level photoemission ascribed to OH species can allow a replacement of V^{4+}=O by O---V^{5+}–OH[87], leaving a slightly lower concentration of V^{4+} centers. Separate studies also confirmed this analysis and further suggested that the V^{4+} concentration is specifically lessened on the V_3 sites of the lattice which are predominantly tetravalent. The oxidation state of the Pt is found as Pt(0) and Pt(II), but is found to be difficult to quantitatively analyses in the small quantities used.

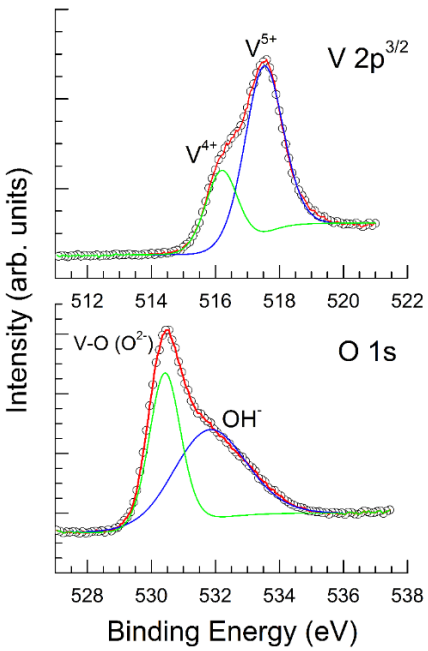

Fig. 8 X-ray photoelectron spectroscopy of the Q1-D complex-intercalated V_2O_5 showing the binding energies for the V $2p^{3/2}$ and O 1s core-levels.

These data confirm that reduction of the vanadium oxide does occur to some extent after incorporation of the Q1-D chains between the bilayer slabs of V_2O_5. The multiplet splitting of V^{5+} and V^{4+} centers from unpaired 3d electrons after intercalation, is 1.33 eV (charge corrected to O 1s), and compares well with the value of 1.17 for V_2O_5 with an oxidation state of 4.2. It is not clear, however, if oxygen vacancies produce a localized reduced vanadium state in the band gap due to the overall reaction, since detailed computational studies are required to define the increased metallic state of the reduced vanadium atoms while being coordinated to the Q1-D complex chains; it is likely that the band

structure is considerably more complex. The values for this system are consistent with reduced V=O (oxygen vacancy defects) in theoretical and experimental investigations of very controlled V_2O_5 surfaces and deposits. The mechanism of oxygen vacancy formation in vanadium oxide has been the subject of intense debate in theoretical studies[88], and its process has been confirmed through numerous spectroscopic and microscopy techniques[89] such as scanning tunnelling microscopy[90], transmission electron microscopy and angle resolved X-ray and ultraviolet photoelectron spectroscopies, among others[91].

In spite of experimental observation of V_2O_5 nanocrystallites in the final film, these centres do not seem to contribute to a change in variable range hopping (VRH) conduction mechanism to Efros-Schlovskii VRH[37, 60] conduction, which has been found in other vanadium oxides where disorder was intentionally induced. Further work will be required to assess any variation in conduction mechanism from these hybrid thin film/nanosheets systems at low (<77 K) temperatures, coupled with electronic structure and molecular dynamics models to more accurately describe the interaction between the host an guest and its detailed influence on the conduction mechanisms at the molecular level that are more difficult to assess in planar device geometries.

4. Conclusions

In summary, this work reports the synthesis and formation of a new layered nanocomposite from a vanadium oxide xerogel and the Q1-D solid complex $K_2Pt(CN)_4$, that exhibits a large conductivity change (a factor of ~1300×) depending on whether transport is across the hybrid nanosheet stacks (through its thickness) or along their layering direction on the substrate. The intercalation of these linear complexes results in a decrease in the hydrated xerogel interlayer spacing without dehydration, and examination of samples after >2 years of ageing allowed analysis of fully crystallized, chemically, structurally and electronically stable films. The mechanism of the directional resistance change was shown to vary from small polaron hoping conduction along the layering direction to more resistive Ohmic transport through the thin film. Further development using lithographically defined top and back-gated 3-terminal devices will examine in more detail the influence of this chemical modification on the electrical properties, focusing on the mechanisms of charge transfer in the Q1-D chain within a polaron conducting host, and in various gated regimes as a thin film device. This work shows that directional conductivity (or resistivity) change is possible using thin films without necessitating a metal-insulator transition or tuning of grain boundary density or other mechanical/chemical features in the composite to vary the conductivity pathway through the material[92]. Scope exists too for synergy in functionalization of semiconducting oxides and electrostatic and thermal control of conduction mechanisms for resistive memory or logic based thin film applications. Further development using the wide range of known organic-inorganic layered materials and oxides might allow for tunable conductors in complementary logic and to study strongly correlated electron effects at oxide interfaces.

Notes and references

[a] *Department of Chemistry, University College Cork, Cork, Ireland*
[b] *Tyndall National Institute, Lee Maltings, Dyke Parade, University College Cork, Cork, Ireland.*
Fax: +353 (0)21 427 4097; Email: c.odwyer@ucc.ie
[c] *Departamento de Ciencias Químicas y Farmacéuticas, Universidad Católica del Norte, Av. Angamos 0610 Antofagasta, Chile*
[d] *Centre for Research on Adaptive Nanostructures and Nanodevices (CRANN), Trinity College Dublin, Dublin 2, Ireland*
[e] *Departamento de Química, Universidad Tecnológica Metropolitana, P.O. Box 9845, Santiago, Chile*
[f] *Center for the Development of Nanoscience and Nanotechnology, CEDENNA, Santiago, Chile*
[g] *Faculdade de Química, Pontifícia Universidade Católica do Rio Grande do Sul, Porto Alegre - RS CEP 90619-900, Brazil*
[h] *Departamento de Química, Facultad de Ciencias, Universidad de Chile, P.O. Box 653, Santiago, Chile*
[i] *Materials & Surface Science Institute, University of Limerick, Limerick, Ireland*
†Electronic Supplementary Information (ESI) available: Supplementary I-V analysis of deposits, optical and SEM images of V_2O_5 layers, TEM analysis of the layered material crystal structure and XPS analysis of the phases. See DOI: 10.1039/b000000x/.
‡ CG acknowledges support from the Irish Research Council from grant no RS/2011/797. The financial support from FONDECYT grant 1131112, CONICYT grant FB0807-CEDENNA, and MSI grant P10-061-F is also acknowledged. DT acknowledges Science Foundation Ireland for financial support under Grant Number 11/SIRG/B2111. VL acknowledges PBCT grant ACT027. COD was supported by Science Foundation Ireland under grant no. 07/SK/B1232a, the UCC Strategic Research Fund, and from the Irish Research Council New Foundations Award 2012.

1. K. Krogmann and H. D. Hausen, *Z. Anorg. Allg. Chem.*, 1968, **67**, 358.
2. S. K. Hurst, L. Spangler, E. H. Abbot, R. Larsen and E. S. Peterson, *Inorg. Chim. Acta*, 2005, **358**, 173.
3. A. Imambekov, T. L. Schmidt and L. I. Glazman, *Rev. Mod. Phys.* , 2012, **84** 1253-1306.
4. M. Bockrath, D. H. Cobden, J. Lu, A. G. Rinzler, R. E. Smalley, L. Balents and P. L. McEuen, *Nature* 1999, **397**, 598-601.
5. R. E. Peierls, Oxford Univ. Press, London, 1955.
6. L. Perfetti, A. Loukakos, M. Lisowski, U. Bovensiepen, H. Berger, S. Biermann, P. S. Cornaglia, A. Georges and M. Wolf, *Phys. Rev. Lett.* , 2006, **97**, 067402.
7. P. Day and A. K. Cheetham, *Solid State Chemistry: Compounds*, Editorial Clarendon Press, Oxford, 1997.
8. A. Noy, *Advanced Materials*, 2011, **23**, 807-820.
9. R. E. Peierls, Oxford Univ. Press, London, 1955, p. p. 108.
10. S. Brown and G. Gruner, *Sci. Am.*, 1994, **270**, 50.
11. A. König, K. Koepernik, R. Schuster, R. Kraus, M. Knupfer, B. Büchner and H. Berger, *Europhys. Lett.*, 2012, **100**, 27002.
12. K. Rossnagel, *J. Phys.: Cond. Matter*, 2011, **23**, 213001.
13. T. E. Mallouk and J. A. Gavin, *Accounts of Chemical Research*, 1998, **31**, 209-217.
14. C. O'Dwyer, V. Lavayen, D. Fuenzalida, H. Lozano, M. A. Santa Ana, E. Benavente, G. Gonzalez and C. M. S. Torres, *Small*, 2008, **4**, 990-1000.
15. C. O'Dwyer, V. Lavayen, S. B. Newcomb, M. A. S. Ana, E. Benavente, G. Gonzalez and C. M. S. Torres, *Journal of the Electrochemical Society*, 2007, **154**, K29-K35.
16. Y. N. Xia, P. D. Yang, Y. G. Sun, Y. Y. Wu, B. Mayers, B. Gates, Y. D. Yin, F. Kim and Y. Q. Yan, *Advanced Materials*, 2003, **15**, 353-389.
17. J. Jin, Y. Wakayama, X. S. Peng and I. Ichinose, *Nature Materials*, 2007, **6**, 686-691.

18. B. J. Scott, G. Wirnsberger and G. D. Stucky, *Chemistry of Materials*, 2001, **13**, 3140-3150.
19. G. Schottner, *Chem. Mater.*, 2001, **13**, 3422.
20. P. J. a. C. Sanchez, *J. Mater. Chem.*, 1996, **6**, 511-525.
21. G. Gannon, C. O'Dwyer, J. A. Larsson and D. Thompson, *J. Phys. Chem. B*, 2011, **115**, 14518–14525.
22. C. O'Dwyer, G. Gannon, D. McNulty, D. N. Buckley and D. Thompson, *Chem. Mater.*, 2012, **24**, 3981–3992.
23. C. R. Kagan, D. B. Mitzi and C. D. Dimitrakopoulos, *Science*, 1999, **286**, 945.
24. D. O'Hare, A. I. Khan, A. Ragavan, B. Fong, C. Markland, M. O'Brien, T. G. Dunbar and G. R. Williams, *Industrial & Engineering Chemistry Research*, 2009, **48**, 10196-10205.
25. M. Giorgetti, S. Passerini, M. Berrettoni and W. H. Smyri, *Journal of Synchrotron Radiation*, 1999, **6**, 743-745.
26. T. Brezesinski, M. Antonietti and B. M. Smarsly, *Adv. Mater.*, 2007, **19**, 1074.
27. H. Fu, Z.-P. Liu, Z.-H. Li, W.-N. Wang and K.-N. Fan, *Journal of the American Chemical Society*, 2006, **128**, 11114-11123.
28. D. Sun, C. W. Kwon, G. Baure, E. Richman, J. MacLean, B. Dunn and S. H. Tolbert, *Adv. Funct. Mater.*, 2004, **14**, 1197.
29. S. Tepavcevic, H. Xiong, V. R. Stamenkovic, X. Zuo, M. Balasubramanian, V. B. Prakapenka, C. S. Johnson and T. Rajh, *ACS Nano*, 2012, **6**, 530.
30. K. K. Banger, Y. Yamashita, K. Mori, R. L. Peterson, T. Leedham, J. Rickard and H. Sirringhaus, *Nat. Mater.*, 2011, **10**, 45-50.
31. M. Sofos, J. Goldberger, D. A. Stone, J. E. Allen, Q. Ma, D. J. Herman, W. W. Tsai, L. J. Lauhon and S. I. Stupp, *Nature Materials*, 2009, **8**, 68-75.
32. Z. W. Pan, Z. R. Dai and Z. L. Wang, *Science*, 2001, **291**, 1947.
33. J. Livage, *Nature Materials*, 2003, **2**, 297-299.
34. C. R. Kagan, D. B. Mitzi and C. D. Dimitrakopoulos, *Science*, 1999, **286**, 945.
35. C.-G. Wu, D. C. DeGroot, H. O. Marcy, J. L. Schindler, C. R. Kannewurf, Y.-J. Liu, W. Hirpo and M. G. Kanatzidis, *Chem. Mater.*, 1996, **8**, 1992-2004.
36. S. S. N. Bharadwaja, C. Venkatasubramanian, N. Fieldhouse, S. Ashok, M. W. Horn and T. N. Jackson, *Appl. Phys. Lett.*, 2009, **94**, 222110
37. A. L. Efros and B. I. Shklovskii, *J. Phys. C*, 1975, **8**, L49.
38. H. W. Jang, D. A. Felker, C. W. Bark, Y. Wang, M. K. Niranjan, C. T. Nelson, Y. Zhang, D. Su, C. M. Folkman, S. H. Baek, S. Lee, K. Janicka, Y. Zhu, X. Q. Pan, D. D. Fong, E. Y. Tsymbal, M. S. Rzchowski and C. B. Eom, *Science*, 2011, **331**, 886-889.
39. J. Mannhart and D. G. Schlom, *Science*, 2010, **327**, 1607-1611.
40. G. Hammerl and N. Spaldin, *Science*, 2011, **332**, 922-923.
41. M. J. Lee, Y. Park, D. S. Suh, E. H. Lee, S. Seo, D. C. Kim, R. Jung, B. S. Kang, S. E. Ahn, C. B. Lee, D. H. Seo, Y. K. Cha, I. K. Yoo, J. S. Kim and B. H. Park, *Adv. Mater.*, 2007, **19**, 3919.
42. J. Nag, E. A. Payzant, K. L. More and R. F. Haglund, *Appl. Phys. Lett.*, 2011, **98**, 251916.
43. S. Biermann, A. Poteryaev, A. I. Lichtenstein and A. Georges, *Phys. Rev. Lett.*, 2005, **94**, 026404.
44. J. M. Baik, M. H. Kim, C. Larson, C. T. Yavuz, G. D. Stucky, A. M. Wodtke and M. Moskovits, *Nano Lett.*, 2009, **9**, 3980-3984.
45. D. Ruzmetov, K. T. Zawilski, V. Narayanamurti and S. Ramanathan, *J. Appl. Phys.*, 2007, **102**, 113715.
46. H. T. Kim, B. G. Chae, D. H. Youn, S. L. Maeng, G. Kim, K. Y. Kang and Y. S. Lim, *New J. Phys.*, 2004, **6**, 52.
47. D. Ruzmetov, G. Gopalakrishnan, C. Ko, V. Narayanamurti and S. Ramanathan, *J. Appl. Phys.*, 2010, **107**, 114516.
48. H. T. Kim, Y. W. Lee, B. J. Kim, B. G. Chae, S. J. Yun, K. Y. Kang, K. J. Han, K. J. Yee and Y. S. Lim, *Phys. Rev. Lett.*, 2006, **97**, 266401.
49. C. O'Dwyer, V. Lavayen, M. A. Santa Ana, S. B. Newcomb, E. Benavente, G. Gonzalez and C. M. S. TorreS, *Physica Status Solidi B-Basic Solid State Physics*, 2006, **243**, 3285-3289.
50. C. O'Dwyer, D. Navas, V. Lavayen, E. Benavente, M. A. Santa Ana, G. Gonzalez, S. B. Newcomb and C. M. S. Torres, *Chemistry of Materials*, 2006, **18**, 3016-3022.
51. C. O'Dwyer, V. Lavayen, D. A. Tanner, S. B. Newcomb, E. Benavente, G. Gonzalez and C. M. S. Torres, *Advanced Functional Materials*, 2009, **19**, 1736-1745.
52. Y. Chen, G. Yang, Z. Zhang, X. Yang, W. Hou and J.-J. Zhu, *Nanoscale*, 2010, **2**, 2131-2138.
53. M. L. Rojas-Cervantes, B. Casal, P. Aranda, M. Savirón, J. C. Galván and E. Ruiz-Hitzky, *Colloid Polym Sci*, 2001, **279**, 990-1004.
54. B. Casal, E. Ruiz-Hitzky, M. Crespin, D. Tinet and J. C. Galván, *J. Chem. Soc. Faraday Trans. I* 1989, **85**, 4167.
55. E. Ruiz-Hitzky, *Chem. Rev.* , 2003, **3**, 88-100.
56. C. J. Brinker, G. C. Frye, A. J. Hurd and C. S. Ashley, *Thin Solid Films*, 1991, **201**, 97.
57. C.-G. Wu, D. C. DeGroot, H. O. Marcy, J. L. Schindler, C. R. Kannewurf, Y.-J. Liu, W. Hirpo and M. G. Kanatzidis, *Chem. Mater.*, 1996, **8**, 1992.
58. V. Lavayen, V. Sanchez, E. Benavente, C. O'Dwyer, C. M. S. Torres, G. Gonzalez and M. A. Santa Ana, *Applied Surface Science*, 2006, **252**, 7941-7947.
59. Y.-J. Liu, J. L. Schindler, D. C. DeGroot, C. R. Kannewurf, W. Hirpo and M. G. Kanatzidis, *Chem. Mater.*, 1996, **8**, 525.
60. N. F. Mott, *J. Non-Cryst. Solids*, 1968, **1**, 1.
61. J. Muster, G. T. Kim, V. Krstic, J. G. Park, Y. W. Park, S. Roth and M. Burghard, *Adv. Mater.*, 2000, **12**, 420.
62. J. B. Goodenough, *Prog. Solid State Chem.* , 1971, **5**, 308.
63. P. W. Anderson, *Phys. Rev.*, 1956, **102**, 1000.
64. C. O'Dwyer, V. Lavayen, D. A. Tanner, S. B. Newcomb, E. Benavente, G. Gonzalez and C. M. S. Torres, *Advanced Functional Materials*, 2009, **19**, 1736-1745.
65. V. Petkov, P. N. Trikalitis, E. S. Bozin, S. J. L. Billinge, T. Vogt and M. G. Kanatzidis, *J. Am. Chem. Soc.*, 2002, **124**, 10157-10162.
66. Y. T., Y. Oka and N. Yamamoto, *Mater. Res. Bull*, 1992, **27**, 669.
67. Y. T., Y. Oka and N. Yamamoto, *J. Mater. Chem.*, 1992, **2**, 331.
68. Y. Wang and G. Z. Cao, *Chemistry of Materials*, 2006, **18**, 2787-2804.
69. S. U. Dunham and E. H. Abbott, *Inorg. Chim. Acta*, 2000, **297**, 72.
70. S. Ding, N. D. Jones and C. A. McDowell, *Solid State Nucl. Magn. Reson.*, 1998, **10**, 205.
71. M. Giorgetti, S. Passerini, W. H. Smyrl and M. Berrettoni, *Inorganic Chemistry*, 2000, **39**, 1514-1517.
72. F. Krumeich, H. J. Muhr, M. Niederberger, F. Bieri, B. Schnder and R. Nesper, *J. Am. Chem. Soc.*, 1999, **121**, 8324.

73. Y.-J. Liu, J. A. Cowen, T. A. Kaplan, D. C. DeGroot, J. L. Schindler, C. R. Kannewurf and M. G. Kanatzidis, *Chem. Mater. 7*, 1995, **7**, 1616-1624.
74. O. Durupthy, N. Steunou, T. Coradin and J. Livage, *J. Phys.Chem. Solids*, 2006, **67**, 944-949.
75. J. Livage, *Coord. Chem. Rev.*, 1998, **178-180**, 999-1018.
76. M. A. S. Ana, E. Benavente, P. Gomez-Romero and G. Gonzalez, *J. Mater. Chem.*, 2006, **16**, 3107–3113.
77. M. Moreno, M. A. S. Ana, G. Gonzalez and E. Benavente, *Electrochim. Acta*, 2010, **55**, 1323–1327.
78. D. B. Williams and C. C. B., *Transmission Electron Microscopy*, Plenum, New York, 1996.
79. L. Abello, E. Husson, E. Repelin and G. Lucazeau, *Spectrochim. Acta, Part A*, 1983, **39**, 641.
80. P. Clauws and J. Vennik, *Phys. Status Solidi B*, 1980, **59**, 469.
81. L. Z.-F., W. Z.-M., X. X.-D., T. Wang and J. Y.-D., *Acta Phys. Sin.*, 2011, **60**, 067302.
82. N. Pinna, M. Willinger, K. Weiss, J. Urban and R. Schogl, *Nano Lett.*, 2003, **3**, 1131.
83. J. Bullot, P. Cordier, O. Gallais, M. Gauthier and J. Livage, *J. Non-Cryst. Solids*, 1984, **68**, 135.
84. G. W. Coulston, E. A. Thompson and N. Herron, *Journal of Catalysis*, 1996, **163**, 122-129.
85. M. Willinger, N. Pinna, D. S. Su and R. Schlogl, *Phys. Rev. B*, 2004, **69**, 155114-155117.
86. M. E. Saleta, C. A. Lopez, M. Granada, H. E. Troiani, R. D. Sanchez, M. Malta and R. M. Torresi, *J. Appl. Phys.*, 2012, **112**, 053912.
87. S. Cheng, H. Hwang and G. E. Maciel, *J. Mol. Struct.*, 1998, **470**, 135.
88. D. O. Scanlon, A. Walsh, B. J. Morgan and G. W. Watson, *J. Phys. Chem. C*, 2008, **112**, 9903.
89. K. Devriendt, H. Poelman, L. Fiermans, G. Creten and G. F. Froment, *Surf. Sci.*, 1996, **352-354**, 750.
90. R. A. Goschke, K. Vey, M. Maier, U. Walter, E. Goering, M. Klemm and S. Horn, *Surf. Sci.* , 1996, **348**, 305.
91. K. Hermann, M. Witko, R. Druzinic, A. Chakrabarti, B. Tepper, M. Elsner, A. Gorschluter, H. Kuhlenbeck and H. J. J. Freund, *Electron Spectrosc. Relat. Phenom.*, 1999, **98-99**, 245.
92. F. Kopnov, G. Leitus, A. Yoffe, I. Feldman, A. M. Panich and R. Tenne, *phys. stat. sol. (b)*, 2006, **243**, 3290.

